

## Capillary Force on a Nanoscale Tip in Dip-Pen Nanolithography

Joonkyung Jang, George C. Schatz, and Mark A. Ratner

*Department of Chemistry, Materials Research Center and Center for Nanofabrication and Molecular Self Assembly, Northwestern University, Evanston, Illinois 60208*

(Received 22 October 2002; published 17 April 2003)

Monte Carlo simulation has been used to characterize the capillary force due to the condensation of a liquid meniscus between a tip with a nanoscale asperity and a flat surface. To consider both hydrophobic and hydrophilic molecules coating the tip as a model of dip-pen nanolithography, tips with various wettabilities are studied. The capillary force due to the meniscus is calculated for various saturations (humidities). We have implemented a thermodynamic integration technique that can project the force into energetic and entropic contributions. In most cases, the force is mainly energetic in origin. At the snap-off separation where the meniscus disappears, the tip feels a significant entropic force at high saturation. Our calculation shows nonmonotonic behavior of the pull-off force as a function of saturation, which is in qualitative accord with experiments.

DOI: 10.1103/PhysRevLett.90.156104

PACS numbers: 68.35.Np, 05.10.Ln, 68.08.Bc

Among the various phase transitions found in geometrically confined systems, *capillary condensation* [1] in particular is important to the recently developed dip-pen nanolithography (DPN) [2]: Under ambient conditions, water vapor condenses to form a liquid meniscus between a sharp (with a nanoscale radius of curvature) atomic force microscope (AFM) tip and a substrate surface. The molecules coated on the tip are then transported through or on the meniscus to the substrate. Previously, we have presented a theoretical analysis of the thermodynamic properties of the liquid meniscus for hydrophobic and hydrophilic AFM tips. The meniscus width and shape were characterized as a function of tip curvature, tip-substrate distance, humidity, and temperature [3].

In DPN (more generally, in any experiment utilizing an AFM-type probe), what is directly observed is the force exerted on the tip by the surface. Under ambient conditions, the *capillary force* due to the water meniscus usually dominates other contributions to the tip-surface interaction, and thus is crucial in determining adhesional and tribological properties of surfaces. There have been many experiments reporting how the capillary force varies with changing humidity [4–6]. Relying on macroscopic theories for fitting the data, these experiments have not provided any microscopic insights into the capillary force. On the theoretical side, most studies [7–11] have focused on slitlike geometries with emphasis on surface force apparatus experiments [12]. A recent theoretical study of the capillary force associated with a nanoscale tip was again based on the macroscopic Kelvin equation [13] and thus lacks microscopic details such as the formation of layers on the surface and fluctuations in the meniscus width [3]. In this Letter, we report the first microscopic Monte Carlo calculation of the capillary force relevant to DPN: the force associated with a nanoscale tip in (near) contact with a surface. We also present a novel methodology for calculating surface forces in lattice models of fluid systems.

As in Ref. [3], we utilize a two-dimensional lattice gas model [14] for water and systematically study the effects of humidity, tip wettability, and tip-substrate distance. The fluid is represented on a square lattice (with a lattice spacing  $l$ ) bounded by an elliptical tip surface and a flat substrate surface (Fig. 1). Each occupied site of our system interacts with its (occupied) nearest neighbor sites with an attractive energy  $\epsilon$ . A fluid particle binds to the tip and substrate surfaces with energies  $b_T$  and  $b_S$ , respectively. Assuming our system is in thermal and phase equilibrium with a bulk reservoir specified by temperature  $T$  and chemical potential  $\mu$ , we utilize grand canonical Monte

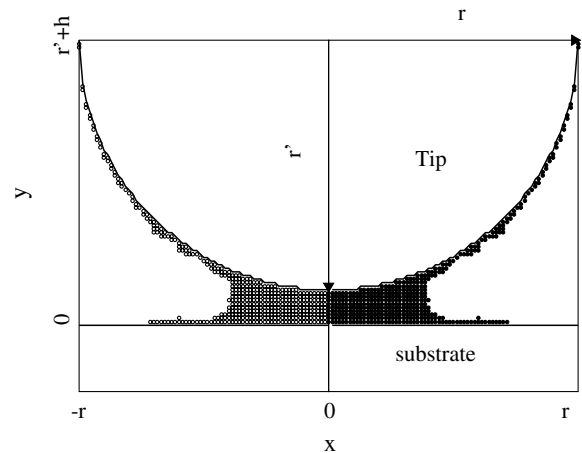


FIG. 1. System geometry and reflecting boundary conditions used in force calculation. The fluid is a two-dimensional square lattice gas confined between a flat substrate surface at  $y = 0$  and an elliptical tip surface with axis lengths of  $r$  and  $r'$  lattice spacings (aspect ratio  $\alpha = r'/r$ ). The tip surface is separated from the substrate by  $h$  lattice spacings. The left part ( $x < 0$ , open circles) is taken to be the mirror image (relative to  $x = 0$ ) of the right ( $x \geq 0$ , black particles). The boundary conditions for  $x > r$  are invoked by taking a mirror image of the system with respect to  $x = r$ .

Carlo (GCMC) simulations (for more details, see Ref. [3]). In this simulation, both energy  $E$  and number of particles  $N$  are variable quantities, and the thermodynamic potential to be minimized is the grand potential  $\Omega = H - TS$ , where  $H$  is the effective energy ( $= E - \mu N$ ) and  $S$  is the entropy.

To emulate the water confined between a gold surface and an AFM tip, we use the following geometric and energetic parameters. The lattice spacing,  $l$ , represents the intermolecular distance in water, which is approximately 3.24 Å [3]. The tip radius parameter  $r$  is defined to make  $r/l = 140$  and, as a result, the simulation box covers 91 nm along the surface. The tip curvature is taken to be  $\alpha = 2$  to mimic a tip with a nanoscale radius of curvature ( $\sim 23$  nm). The nearest neighbor attraction  $\epsilon$  for water is roughly 20 kJ/mol and the water-gold binding energy is about 60 kJ/mol [15]. We thus take  $b_S/\epsilon = 3$  in our simulation, which makes the fluid completely wet the substrate [16]. To examine both hydrophilic and hydrophobic tips in DPN, we consider three different tip binding energies,  $b_T/\epsilon = 3, 0.75,$  and  $0.25$ , whose wetting properties are *completely wetting* (CW), *partially wetting* (PW), and *partially drying* (PD), respectively [16]. The wetting tips (the CW and PW tips) correspond to hydrophilic tips, and the PD tip to a hydrophobic tip. The temperature was set to simulate water at room temperature (300 K),  $T/T_c = 0.46$ , where  $T_c$  is the bulk critical temperature for the lattice gas [ $= (\epsilon/2k_B)/\ln(1 + \sqrt{2})$ ] [14]. Identifying  $T_c$  as the water critical temperature (647.30 K) gives  $\epsilon = 9.5$  kJ/mol for water. Simulations are run by varying the tip-substrate distance as well as the *saturation* (which corresponds to relative humidity for water) defined as  $\text{sat} = \exp[(\mu - \mu_c)/k_B T]$ , where  $\mu_c$  is the chemical potential at the bulk gas-liquid transition ( $= -2\epsilon$ ) [14].

Evaluation of the capillary force from simulation follows a lengthy, indirect route as is now discussed. This is due to the fact that the gradient of the molecular interaction is not defined in our lattice system, and thus virial-type (involving averages of the gradient of interaction potential) expressions [10,11] for forces cannot be applied. Therefore, we use the following expression for the force at the tip-substrate distance  $h$  [8,9]:

$$F(h) = -\left(\frac{\partial \Omega}{\partial h}\right)_{\mu, T} - p\left(\frac{\partial V}{\partial h}\right)_{\mu, T}, \quad (1)$$

where  $V$  is the system volume, and  $p$  is the pressure of the bulk system. To obtain  $\Omega$  and  $p$  from simulation, we adopt a thermodynamic integration method which has been widely used in locating the exact transition point for gas-liquid phase transitions [17,18]. Specifically, we utilize the following relation [17]:

$$\beta \Omega = \beta_0 \Omega_0 + \int_{\beta_0}^{\beta} H(\beta) d\beta \quad (\beta = 1/k_B T), \quad (2)$$

where the zero subscript represents a reference state whose grand potential is known exactly. To evaluate the

grand potential at the desired temperature  $\beta$ , we choose infinite temperature ( $\beta_0 = 0$ ) as the reference state and discretize the integral in Eq. (2) by using Simpson's rule. The potential gradient in Eq. (1) is then evaluated as  $(\partial \Omega / \partial h) = [\Omega(h+l) - \Omega(h)]/l$ . The bulk pressure,  $p$  (note  $p$  is the bulk grand potential per unit volume), is calculated by running separate simulations for a bulk system and using the same thermodynamic integration technique described above. A nice feature of evaluating  $\Omega$  directly is that the force can be naturally divided into energetic and entropic contributions, as the grand potential is the sum of an energy ( $H$ ) and entropy ( $TS$ ). We note that Fisher [19] has considered energetic and entropic contributions (which become identical at  $T_c$ ) to the surface energies of droplets in a homogeneous gas. In contrast, the current analysis (see below) focuses on energetic and entropic contributions to the force (gradient of energy with respect to  $h$ ). Also, the droplets in this study arise from inhomogeneous geometric confinement, rather than spontaneous nucleation in the bulk.

For completeness, we explored another thermodynamic integration method for calculating the capillary force. A useful expression for the force was derived by Ash *et al.* [20]:

$$F(\mu, h, T) - F(\mu = -\infty, h, T) = \int_{-\infty}^{\mu} \left(\frac{\partial N_{\text{ex}}}{\partial h}\right)_{\mu'} d\mu', \quad (3)$$

where  $N_{\text{ex}}$  is the excess number of molecules of our system relative to that in a bulk system with the same volume  $V$ . We call the above equation the  $\mu$  integration method as opposed to the  $T$  integration method [Eq. (2)]. Starting from a sufficiently low chemical potential which should give zero force, we discretize the integral in Eq. (3) following a procedure similar to that done in discretizing Eq. (2).

The force-distance curves for the PW tip at several saturations are drawn in Fig. 2. All the forces reported in this paper are in units of  $\epsilon/l$  ( $\sim 49$  pN for water), and are assumed to be obtained from the  $T$  integration method if we do not specify which method is used. As can be seen in the figure, the closest possible distance  $h = l$  is the most unfavorable. When the tip is too close to the substrate, it actually displaces the molecules out of the tip-substrate contact region, reducing the total adhesive energy of the liquid meniscus. The most stable system geometry is the case where  $h/l = 2$ . The above observations are made for all the tip wettabilities and saturations considered in our simulation. The repulsive nature of the capillary force at the shortest distance cannot be captured by the macroscopic thermodynamic approach [13]. As the tip recedes from the substrate, the meniscus disappears and the force approaches zero. At low saturations (20% and 40%), the force-distance curve has a narrow well located at  $h/l = 2$  and the force goes to zero at short distances (at  $h$  less than  $7l$ ). As the saturation increases,

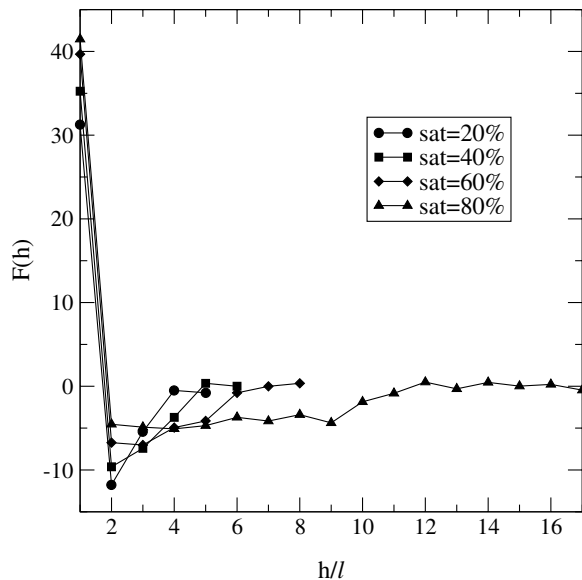


FIG. 2. The capillary force,  $F(h)$ , vs the tip-substrate distance  $h$  for the PW tip at various saturations. As saturation increases, the narrow dip located at  $h = 2l$  in the force curve broadens and decreases in depth. The force is attractive (repulsive) if it is negative (positive). In this and all the following figures, lines are drawn as guides to the eyes.

the narrow well in the force curve becomes broad and plateaulike, and the force vanishes rather smoothly as  $h$  increases. The above trends are also found for the PD and CW tips, and are physically reasonable: As the humidity increases, the tip is wetted more completely, and withdrawing the tip from the substrate involves gradual shedding of many layers of water from the tip. This accounts for both the breadth and the shallowness of the higher humidity plots in Fig. 2.

As we pointed out earlier, the  $T$  integration technique allows us to divide the force into energetic and entropic parts. Such a projection is done in Fig. 3 for the CW tip at low and high saturations. At most tip-substrate distances, the entropic force is negligible and the energetic contribution dominates the capillary force. At the snap-off distance ( $h/l = 12$  for saturation 85%) for high saturation, however (Fig. 3, bottom), the entropic force is comparable to the energetic force. As the meniscus snaps off, the tip experiences a repulsive entropic force which drives the transition from liquid meniscus to a gaslike state. This is almost perfectly counterbalanced by an attractive force arising from loss of adhesive energy which resists the energetic destabilization, such that the net force varies smoothly with separation. We performed projections similar to Fig. 3 for the PD, PW, and CW tips for saturations ranging from 5% to 90%. The entropic forces are found negligible at all saturations for the PD tip, at saturations below 80% for the PW tip, and at saturations below 75% for the CW tip.

The magnitude of the maximum attractive force in the force-distance curve (e.g., the force at  $h/l = 2$  in Fig. 2) is

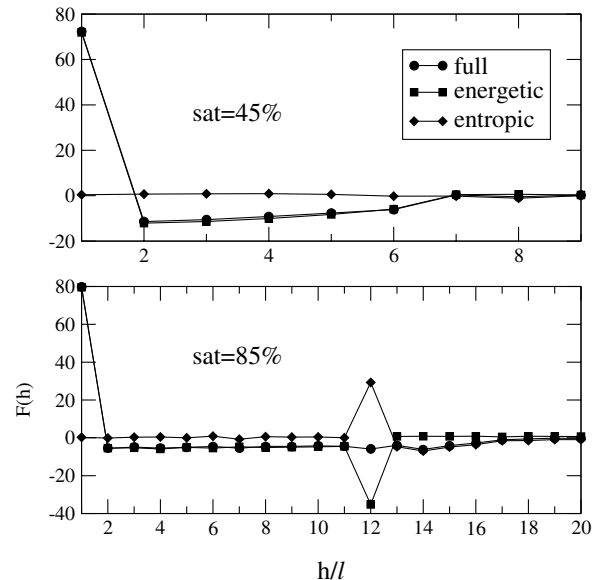


FIG. 3. The capillary force  $F(h)$  and its projection onto the energetic and entropic contributions for the CW tip at low (45%) and high (85%) saturations. The entropic force is negligible in most cases. At the snap off of meniscus for high saturation [ $h/l = 12$ , bottom], however, it becomes significant and accompanied by an energetic force of nearly the same magnitude in the opposite direction.

called the *pull-off force* [4]. In Fig. 4, we plot how the pull-off force varies with saturation for different tip wettabilities. The  $\mu$  integration method, Eq. (3), yields nearly identical pull-off forces to those obtained by using the  $T$  integration method. Overall, the pull-off force rises as we increase the tip wettability: The average forces in the range of saturations between 5% and 80% are 3.3, 9.2, and 13.4 (in physical dimensions relevant to water, these are 0.16, 0.45, and 0.66 nN) for the PD, PW, and CW tips, respectively. The figure reveals that the pull-off force quickly grows from zero at extremely low saturation to a maximum at approximately 0.06% saturation for the PD and PW tips and at 0.012% for the CW tip. This means that a liquid meniscus forms at low saturation and broadens as saturation increases. This broadening leads to an increase in the pull-off force at low saturation. Then, at higher saturation, the force diminishes slowly with increasing saturation.

The pull-off force is often reported experimentally [4–6] as a function of humidity. The qualitative behavior of force vs saturation found in our simulation is in accord with some of experiments (specifically, the forces between a hydrophilic  $\text{Si}_3\text{N}_4$  tip and a mica surface [4] and between a hydrophilic tip and a silicon surface [5]). The saturation at which the pull-off force peaks, however, is small compared to the experimental values ( $\sim 20\%$  [4] and  $\sim 70\%$  [5]). This is probably due to the rather strong fluid-substrate and fluid-tip interactions used in the calculations. When we used a less strong fluid-surface interaction, the force reaches a maximum at a higher

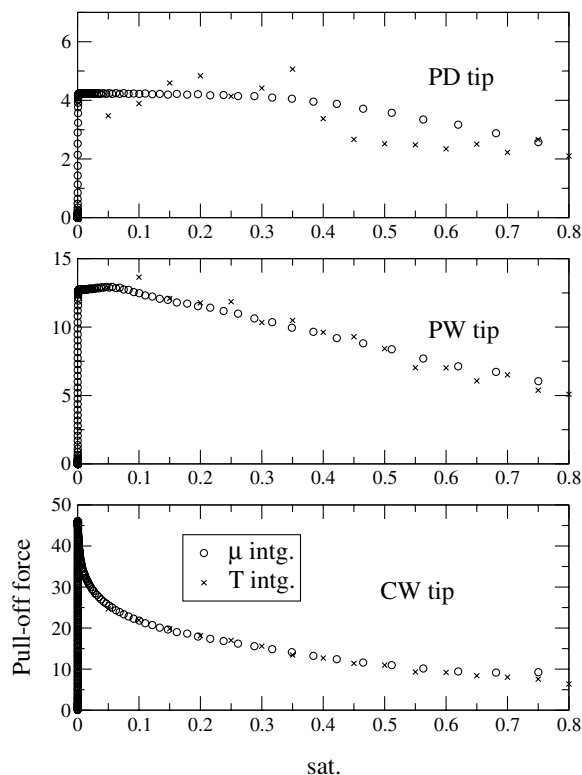


FIG. 4. The saturation dependence of the pull-off force for different tip wettabilities. The results from two different thermodynamic integration techniques are plotted for comparison. At extremely low saturation, the force increases with increasing saturation up to a peak. Further increases in saturation lead to a slow decrease.

saturation. For example, for  $b_S/\epsilon = 2$  and  $b_T/\epsilon = 0.25$ , the maximum pull-off force is located at 20% saturation. Our pull-off forces are hundreds of pNs in magnitude at most which is ten to hundred times less than typical experimental pull-off forces of several nN [4–6]. This is because our two-dimensional simulation underestimates the force arising from the three-dimensional liquid meniscus. We can obtain a rough estimate of the three-dimensional force by assuming it is proportional to the number of molecules in the meniscus. Thus, the force in three dimensions is approximated as the corresponding two-dimensional force times the ratio of numbers of molecules in the three- and two-dimensional menisci. Our three-dimensional simulation (using the same energetic parameters as in this Letter) [21] yields a number ratio of 116 on average. This explains the nearly 2 orders of magnitude difference between our two-dimensional forces and typical experimental values.

In summary, we have presented the first GCMC calculation of the capillary force for a nanoscale tip interacting with a flat surface. To examine both hydrophilic and hydrophobic tips such as are used in DPN, tips with

different wettabilities are simulated. Based on a two-dimensional lattice gas model, we studied the capillary force by systematically varying the tip-substrate distance and saturation. We have also presented novel methods to calculate the force from the simulation, and we have been able to decompose the force into energetic and entropic parts. We can certainly think of a more sophisticated version of our force calculation; i.e., a three-dimensional lattice gas simulation [21] and/or including van der Waals forces between solid surfaces. The current calculation based on a simple model, however, seems to catch the characteristics of the experimental pull-off forces.

This research was supported by AFOSR MURI Grant No. F49620-00-1-0283 and by the National Science Foundation. We thank Chad Mirkin and Seunghun Hong for valuable discussions.

- 
- [1] P. Rocken and P. Tarazona, *J. Chem. Phys.* **105**, 2034 (1996).
  - [2] R. D. Piner *et al.*, *Science* **283**, 661 (1999); S. Hong and C. A. Mirkin, *Science* **288**, 1808 (2000).
  - [3] J. Jang, G. C. Schatz, and M. A. Ratner, *J. Chem. Phys.* **116**, 3875 (2002).
  - [4] L. Xu *et al.*, *J. Phys. Chem. B* **102**, 540 (1998).
  - [5] M. He *et al.*, *J. Chem. Phys.* **114**, 1355 (2001).
  - [6] T. Thundat *et al.*, *Surf. Sci. Lett.* **294**, 939 (1993).
  - [7] J. E. Lane and T. H. Spurling, *Aust. J. Chem.* **33**, 231 (1980).
  - [8] R. Evans and U. Marini Bettolo Marconi, *J. Chem. Phys.* **86**, 7138 (1987).
  - [9] L. J. Douglas Frink and F. van Swol, *J. Chem. Phys.* **106**, 3782 (1997).
  - [10] W. J. van Megen and I. K. Snook, *J. Chem. Phys.* **74**, 1409 (1981).
  - [11] J. J. Magda, M. Tirrell, and H. T. Davis, *J. Chem. Phys.* **83**, 1888 (1985).
  - [12] J. N. Israelachvili and G. E. Adams, *J. Chem. Soc., Faraday Trans. 1* **74**, 975 (1978).
  - [13] T. Stifter, O. Marti, and B. Bhushan, *Phys. Rev. B* **62**, 13 667 (2000).
  - [14] T. L. Hill, *Statistical Mechanics* (McGraw-Hill, New York, 1956), Chap. 7.
  - [15] P. A. Thiel and T. E. Madey, *Surf. Sci. Rep.* **7**, 211 (1987).
  - [16] R. Pandit, M. Schick, and M. Wortis, *Phys. Rev. B* **26**, 5112 (1982).
  - [17] B. K. Peterson and K. E. Gubbins, *Mol. Phys.* **62**, 215 (1987).
  - [18] K. Binder and D. P. Landau, *J. Chem. Phys.* **96**, 1444 (1992).
  - [19] M. E. Fisher, *Physics* **3**, 255 (1967); *J. Appl. Phys.* **38**, 981 (1967); *Rep. Prog. Phys.* **30**, 615 (1967).
  - [20] S. G. Ash, D. H. Everett, and C. Radke, *Faraday Trans. II* **69**, 1256 (1973).
  - [21] J. Jang, G. C. Schatz, and M. A. Ratner (to be published).